A Stabilized ES-FEM for Incompressible flow based on Quasi-implicit Characteristic-based Polynomial Pressure Projection

***† Chen Jiang [1], Xu Han [1], G.R. Liu[2,3]**

[1]State Key Laboratory of Advanced Technology of Design and Manufacturing for Vehicle Body, Hunan University, P.R. China, 410082

[2] Part-time Consultant Professor, State Key Laboratory of Advanced Technology of Design and Manufacturing for Vehicle Body, Hunan University, P.R. China, 410082

[3] Department of Aerospace Engineering and Engineering Mechanics, University of Cincinnati, 2851 Woodside Dr, Cincinnati, OH 45221, USA

*Presenting author: jiangchen2007@hotmail.com

†Corresponding author: hanxu@hnu.edu.cn

Abstract

In this paper, a stabilized edge-based smoothed finite element method (ES-FEM) is proposed to solve incompressible fluid flow problems. To stabilize the convection caused oscillation, characteristic-based method is employed. To stabilize the pressure caused oscillation, the polynomial pressure projection (P3) is used. The proposed stabilization is denoted as CBP3 scheme. One excellent merit of CBP3 scheme stabilization is that it suits for all types of element, even for the simplest 3-node triangular element. The CBP3 scheme implemented into ES-FEM with T3 element is denoted as CBP3/ES-FEM-T3. To verify proposed CBP3 scheme and check its stability, the benchmark, Taylor-Green vortex, is calculated. As a comparison, this benchmark is also calculated by CBP3/FEM-T3. From the solutions of CBP3/FEM-T3 and CBP3/ES-FEM-T3, CBP3 scheme is proved with ability to stabilize FEM and ES-FEM. The convergence studies carried out reveal that CBP3/ES-FEM-T3 beats CBP3/FEM-T3 on accuracies of both velocity and pressure.

Keywords: ES-FEM, Chracteristic-based method, Polynomial pressure projection, Triangular element, Incompressible laminar flow

Introduction

In solid mechanics, the edge-based smoothed finite element method (ES-FEM) has been proven by vast literature [1–5] with much better accuracy and convergence than FEM when using T3 element. Due to the gradient smoothing using edge-based smoothing domain, the strain distribution of ES-FEM in T3 mesh of whole system is smoother than FEM. Therefore, ES-FEM can soft the stiff behavior of T3 element to achieve better solution. Since T3 element can discretize complex geometry by well-developed unstructure mesh generators, one technique which can improve standard FEM T3 element, such as ES-FEM, will be welcomed by engineers.

As a result, it is also attractive to exploit the benefits of ES-FEM in fluid dynamics. The motivation of this paper is to extend ES-FEM using T3 element to solve laminar flow. But unlike the solid governing equation which is self-adjoint Laplace type equation, the Navier-Stokes equations are non self-adjoint. This non self-adjoint feature is derived from the nonlinear convection of fluid flow. Previous investigations about standard Galerkin weighted residual method, such as FEM, for Navier-Stokes equations [6] have shown the spatial oscillation. The ES-FEM also has to face this convection caused oscillation. On the other hand, ES-FEM should also equip with suitable stabilization for pressure oscillation in incompressible flow. The reason why first calculates incompressible laminar flow using ES-FEM is that compressible flow is quite complicate in physics, such as shock waves and high Reynolds number. Usually, incompressible constraint is circumvented by selective S-FEM in solid mechanics. This time, the selective S-FEM approach is not applicable due to the fully incompressibility shown in fluid material behavior. Previous study made by the authors using selective reduced integration of 4-node quadrilateral elements has demonstrated bulk viscosity (analogous to bulk modulus in solid mechanics) must reach to 10e8 times of shear dynamic viscosity to obtain satisfied results. But selective S-FEM shown very violent oscillation in pressure under that high penalty factor.

Therefore, good convection and pressure stabilizations are the prerequisites for successfully using ES-FEM to solve fluid flows. Besides, the potential stabilizations must be friendly to T3 element. We do can successfully solve fluid flows by using higher order elements with easy-to-create unstructured mesh. However, higher order elements, such as 6-node triangular element, consume much more computation resources than T3 elements. Another consideration is that people will not have the impetus to add gradient smoothing to the quite accurate higher order elements. In this paper, we chose widely used characteristic-based method proposed by Zienkiewicz [7] as convection stabilization. On the pressure stabilization, the polynomial pressure projection proposed (P3) by Dohrmann and Bochev [8] is deployed. This P3 pressure stabilization has been demonstrated appropriate for any element type for any level of incompressiblity, including simplest T3 element. In its previous cooperation with S-FEMs for solid mechanics and Stokes flow, P3 stabilization can further soft the behaviors of FEM and S-FEM. Especially, ES-FEM with P3 stabilization outperformed FEM and other S-FEMs for incompressible solid problems using T3 element. Combine aforementioned two stabilizations, we proposed a new stabilization scheme named as Characteristic-based Polynomial Pressure Projection (CBP3). With this CBP3 scheme, FEM and ES-FEM should able to solve incompressible laminar flow.

The rest of the paper is structured as following. The second section introduces the governing equations of incompressible laminar flow. The third section is the brief derivations of CBP3 scheme. The following section describes the merge of CBP3 into ES-FEM. The forth section is the case studies to access the accuracy of proposed methods. In the last section, conclusions are drawn.

Governing equations

If flow is incompressible without heat transfer, the dimensional conservative N-S equations can be simplified to:

$$\begin{cases} \dfrac{\partial v_i}{\partial x_i} = 0, \\ \dfrac{\partial v_i}{\partial t} + \dfrac{\partial}{\partial x_j}(v_j v_i) = -\dfrac{1}{\rho}\dfrac{\partial p}{\partial x_i} + \dfrac{\partial \tau_{ij}}{\partial x_j} + g_i. \end{cases} \tag{1}$$

In which, p is the fluid pressure, v_i is the i-th component of fluid velocity, ρ is the fluid density which is a constant in incompressible flow, g_i is the gravity acceleration, and τ_{ij} is the deviatoric stresses in the fluid:

$$\tau_{ij} = \frac{\mu}{\rho}\left(\frac{\partial v_i}{\partial x_j} + \frac{\partial v_j}{\partial x_i} - \frac{2}{3}\frac{\partial v_k}{\partial x_k}\delta_{ij}\right). \tag{2}$$

where, μ is the fluid dynamic (shear) viscosity and δ_{ij} is the Kronecker delta.

The boundary conditions of N-S equations are the Velocity Boundary Condition (VBC), the Pressure Boundary Condition (PBC) and Traction Boundary Condition (TBC) as below. Meanwhile, the Initial Condition (IC) is also presented below.

$$\begin{aligned} &VBC: v_i = \overline{v}_i, \text{ on } \Gamma_v. \\ &PBC: p = \overline{p}, \text{ on } \Gamma_p. \\ &TBC: t_i = n_j\sigma_{ij} = \overline{t}_i, \text{on } \Gamma_t. \\ &IC: v_i^0 = \overline{v}_i^0,\ p^0 = \overline{p}^0. \end{aligned} \tag{3}$$

where $\Gamma_v \cup \Gamma_t = \Gamma$ and $\Gamma_v \cap \Gamma_t = 0$.

Characteristic-based polynomial pressure projection scheme

Characteristic-based stabilization

When using Galerkin weighted residual numerical methods, like FEM, for N-S equation, the nonlinear non-self-adjoint convection term will cause the numerical oscillation. Since ES-FEM is also based on Galerkin weighted residual method, the characteristic-based stabilization is applied in this paper to cure the convection instability.

In this study, we select the Characteristic-based stabilization which leads to a Characteristic-Galerkin (CG) scheme. This method has a very solid mathematical background which will be demonstrated on one-dimensional scalar convection-diffusion equation,

$$\frac{\partial \phi}{\partial t} + \underset{convective}{U\frac{\partial \phi}{\partial x}} - \underbrace{\frac{\partial}{\partial x}\left(k\frac{\partial \phi}{\partial x}\right)}_{diffusive} + Q = 0 \tag{4}$$

where ϕ is a scalar quantity being transported by the velocity U , and k is the diffusion coefficient.
If we change above equation into a new coordinate system x' which is defined as

$$dx' = dx - Udt \tag{5}$$

Because a physical quantity must not vary if we change our coordinate system, we can get

$$\phi(x,t) = \phi(x',t) \tag{6}$$

Then, we can get following relation

$$\frac{\partial \phi(x,t)}{\partial t} = \frac{\partial \phi(x',t)}{\partial t} + \frac{\partial \phi(x',t)}{\partial x'}\frac{\partial x'}{\partial t} = \frac{\partial \phi(x,t)}{\partial t} - U\frac{\partial \phi(x',t)}{\partial x'} \tag{7}$$

Substitute above relation into Eq.(1.6), we can simplify it at new coordinate system as

$$\frac{\partial \phi}{\partial t} - \frac{\partial}{\partial x'}\left(k\frac{\partial \phi}{\partial x'}\right) + Q(x') = 0 \tag{8}$$

In above equation, it has no convective term any more in this new coordinate system. Furthermore, the equation becomes self-adjoint.

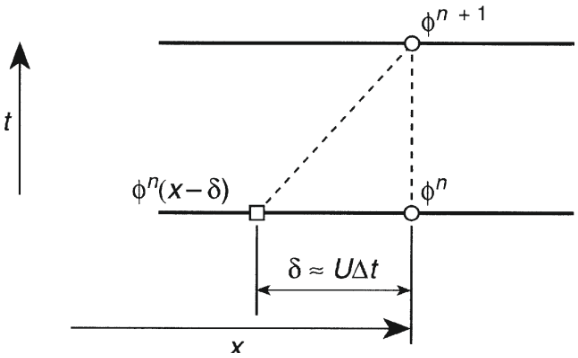

Figure 1. The simple explicit characteristic-Galerkin procedure [9].

We should also pay attention to the new coordinate system on characteristic direction is updated at every time step. The meaning of updating coordinate system is our Euler fluid mesh must moves like a Lagrangian solid mesh. However, this mesh updating is time consuming and will distort mesh. Thus, a simple explicit characteristic-Galerkin procedure was first proposed in 1984 [10] by using the local Taylor expansion on characteristic directions as Figure 1. The detail derivation of this explicit characteristic-Galerkin procedure can be found in reference [6]. We simply write down its final form with Euler time integration,

$$\begin{aligned}\Delta\phi = \phi^{n+1} - \phi^{n} &= -\Delta t\left[U^{n}\frac{\partial\phi}{\partial x} - \frac{\partial}{\partial x}\left(k\frac{\partial\phi}{\partial x}\right) + Q\right]^{n} \\ &+ \frac{\Delta t^{2}}{2}U^{n}\frac{\partial}{\partial x}\left[U^{n}\frac{\partial(\phi)}{\partial x} - \frac{\partial}{\partial x}\left(k\frac{\partial\phi}{\partial x}\right) + Q\right]^{n}.\end{aligned} \tag{9}$$

Its extension to multi-dimensional can be straightforwardly written as

$$\begin{aligned}\Delta\phi = \phi^{n+1} - \phi^{n} &= -\Delta t\left[\frac{\partial U_{j}\phi}{\partial x_{j}} - \frac{\partial}{\partial x_{i}}\left(k\frac{\partial\phi}{\partial x_{i}}\right) + Q\right]^{n} \\ &+ \frac{\Delta t^{2}}{2}U_{k}^{n}\frac{\partial}{\partial x_{k}}\left[\frac{\partial(U_{j}\phi)}{\partial x_{j}} - \frac{\partial}{\partial x_{i}}\left(k\frac{\partial\phi}{\partial x_{i}}\right) + Q\right]^{n}.\end{aligned} \tag{10}$$

Similar procedures can be conducted for incompressible N-S equations as Eq.(1). Here, we only present the final form of explicit characteristic-Galerkin scheme for N-S equations with Euler time integration.

$$\begin{aligned}v_{i}^{n+1} - v_{i}^{n} &= \Delta t\left[\underbrace{-\frac{\partial(v_{j}v_{i})}{\partial x_{j}}}_{convective}\underbrace{-\frac{1}{\rho}\frac{\partial p}{\partial x_{i}} + \frac{1}{\rho}\frac{\partial\tau_{ij}}{\partial x_{j}}}_{diffusive} + g_{i}\right]^{n} \\ &\underbrace{-\frac{\Delta t^{2}}{2}v_{k}\frac{\partial}{\partial x_{k}}\left[-\frac{\partial(v_{j}v_{i})}{\partial x_{j}} - \frac{1}{\rho}\frac{\partial p}{\partial x_{i}} + \frac{1}{\rho}\frac{\partial\tau_{ij}}{\partial x_{j}} + g_{i}\right]^{n}}_{stabilization}.\end{aligned} \tag{11}$$

If calculate the diffusive terms at n+1 time step to the left side of equation, we can achieve the quasi-implicit characteristic-Galerkin scheme as below

$$\begin{aligned} &\underbrace{v_i^{n+1} + \frac{1}{\rho}\frac{\partial p^{n+1}}{\partial x_i} - \frac{1}{\rho}\frac{\partial \tau_{ij}^{n+1}}{\partial x_j}}_{diffusive} = v_i^n + \Delta t\left[-\underbrace{\frac{\partial\left(v_j v_i\right)}{\partial x_j}}_{convective}\right]^n + g_i \\ &\underbrace{-\frac{\Delta t^2}{2} v_k \frac{\partial}{\partial x_k}\left[-\frac{\partial\left(v_j v_i\right)}{\partial x_j} - \frac{1}{\rho}\frac{\partial p}{\partial x_i} + \frac{1}{\rho}\frac{\partial \tau_{ij}}{\partial x_j} + g_i\right]^n}_{stabilization}. \end{aligned} \tag{12}$$

Due to only diffusive terms are calculated implicitly, this scheme is denoted as quasi-implicit scheme.

Characteristic-Galerkin semi-discretized form

Interpolate the velocity and pressure using shape function Φ,

$$v_i(\mathbf{x}) = \sum_{I=1}^{N_n} \Phi(\mathbf{x}_I) v_i(\mathbf{x}_I) = \sum_{I=1}^{N_n} \Phi_I v_{Ii},\ p(\mathbf{x}) = \sum_{I=1}^{N_n} \Phi(\mathbf{x}_I) p(\mathbf{x}_I) = \sum_{I=1}^{N_n} \Phi_I p_I \tag{13}$$

where N_n is total number of nodes in the model, $\Phi(\mathbf{x}_I)$ is the shape function of node *I*, $v_i(\mathbf{x}_I)$ is the velocity of node *I*.

Combine time discretized momentum equation Eq.(12) with the continuity equation in Eq.(1), the semi-discretized weak form is directly provided as below

$$\begin{bmatrix} \dfrac{M_{IJ}}{\Delta t} + K_{IJ} & -Q_{IiJ} \\ -G_{IJi} & 0 \end{bmatrix} \begin{bmatrix} v_{Ji}^{n+1} \\ p_J^{n+1} \end{bmatrix} = \begin{bmatrix} M_{IJ}\dfrac{v_{Ji}^n}{\Delta t} - C_{IJ}^n v_{Ji}^n - \dfrac{\Delta t}{2} H_{IJ}^n v_{Ji}^n + f_{Ii}^t + f_{Ii}^{\mathrm{g}} \\ 0 \end{bmatrix} \tag{14}$$

where

$$\begin{aligned} &M_{IJ} = \int_\Omega \rho \Phi_I \Phi_J \mathrm{d}\Omega, [C]_{IJ}^n = \int_\Omega \rho \Phi_I \frac{\partial\left(v_j^n \Phi_J\right)}{\partial x_j}\mathrm{d}\Omega, \\ &[K]_{IJ} = \int_\Omega \mathbf{B}_I^T \mathbf{D}_\mu \mathbf{B}_J \mathrm{d}\Omega, [H]_{IJ}^n = \int_\Omega \frac{\partial(v_k^n \Phi_I)}{\partial x_k}\rho\frac{\partial(v_j^n \Phi_J)}{\partial x_j}\mathrm{d}\Omega, \\ &[Q]_{IiJ} = \int_\Omega \rho \frac{\partial\left(\Phi_I\right)}{\partial x_i}\Phi_J \mathrm{d}\Omega, [G]_{IJi} = \int_\Omega \rho \Phi_I \frac{\partial\left(\Phi_J\right)}{\partial x_i}\mathrm{d}\Omega, \\ &[f]_{Ii}^{\mathrm{g}} = \int_\Omega \Phi_I \rho g_i \mathrm{d}\Omega, [f]_{Ii}^t = \int_\Gamma \Phi_I \left(\tau_{ij}^n\right) n_j \mathrm{d}\Gamma. \end{aligned} \tag{15}$$

In above equation,

$$\mathbf{B}_I = \begin{bmatrix} \frac{\partial \Phi_I}{\partial x} & 0 \\ 0 & \frac{\partial \Phi_I}{\partial y} \\ \frac{\partial \Phi_I}{\partial y} & \frac{\partial \Phi_I}{\partial x} \end{bmatrix}, \ \mathbf{D}_u = \mu \begin{bmatrix} 2 & 0 & 0 \\ 0 & 2 & 0 \\ 0 & 0 & 1 \end{bmatrix}. \tag{16}$$

Although Eq.(14) is standard weak form for quasi-implicit characteristic-Galerkin scheme, its lower diagonal term of left side matrix is zero which doesn't circumvent the LBB restriction for incompressibility. Hence, directly using Eq.(14) will cause pressure locking or instability.

Polynomial pressure projection

Previous widely used technique to satisfy LBB condition is the Taylor-Hood element [11], using higher order element for velocity and one order lower element for pressure. However, Taylor-Hood elements introduced much more degree of freedoms than equal-order elements for both velocity and pressure. Another widely used approach is the selective reduced integration. This approach has limitation on the element type, usually not applicable for simplest linear triangles and tetrahedrons.

A relatively new pressure stabilization, so called polynomial pressure projection (P3), has been proposed by Dohrmann and Bochev [8]. This very potential technique has been demonstrated its capability to circumvent LBB restriction in incompressible Stokes equation using equal-order shape function for velocity and pressure.

The details of derivation of P3 stabilization can be found in reference [8] and [12]. The implementation of P3 stabilization is adding a stabilization term in weak form Eq.(14) as following

$$\begin{bmatrix} \frac{M_{IJ}}{\Delta t} + K_{IJ} & -Q_{IiJ} \\ -G_{IJi} & -V_{IJ} \end{bmatrix} \begin{bmatrix} v_{Ji}^{n+1} \\ p_J^{n+1} \end{bmatrix} = \begin{bmatrix} M_{IJ} \frac{v_{Ji}^n}{\Delta t} - C_{IJ}^n v_{Ji}^n - \frac{\Delta t}{2} H_{IJ}^n v_{Ji}^n + f_{Ii}^t + f_{Ii}^g \\ 0 \end{bmatrix} \tag{17}$$

where V_{IJ} is the P3 stabilization term. This term V_{IJ} is calculated on each element as below

$$V_{IJ} = \sum_{i=1}^{Ne} \int_{\Omega_e} \frac{\alpha}{\mu} \left(\Phi_I \Phi_J - h_I h_J \right) \mathrm{d}\Omega \tag{18}$$

where h_I is the one order lower polynomial interpolation than shape function Φ_I, α is the parameter of P3 stabilization. In the 3-node triangular element which is used in this paper, the pressure projection for an element is just the average pressure as below

$$\breve{p} = \frac{1}{3}\left(\tilde{p}_1 + \tilde{p}_2 + \tilde{p}_3 \right) \tag{19}$$

where $\breve{p}$ is the pressure projection, $\tilde{p}_i$ is the pressure of i-th node.

Correspondingly, the P3 stabilization term V_{IJ} for 3-node triangular element is given as below

$$V_{IJ} = \frac{\Delta\alpha}{12\mu}\begin{bmatrix} 2 & 1 & 1 \\ 1 & 2 & 1 \\ 1 & 1 & 2 \end{bmatrix} - \frac{\Delta\alpha}{9\mu}\begin{bmatrix} 1 & 1 & 1 \\ 1 & 1 & 1 \\ 1 & 1 & 1 \end{bmatrix} = \frac{\Delta\alpha}{36\mu}\begin{bmatrix} 2 & -1 & -1 \\ -1 & 2 & -1 \\ -1 & -1 & 2 \end{bmatrix} \tag{20}$$

Now, back to Eq.(17), its left side system matrix is positive definite leading to solution for any interpolation of velocity and pressure fields. Since the projected pressure is k-1 order lower than velocity of k order, the mixed patch condition is also satisfied.

Edge-based smoothed finite element method with CBP3 scheme

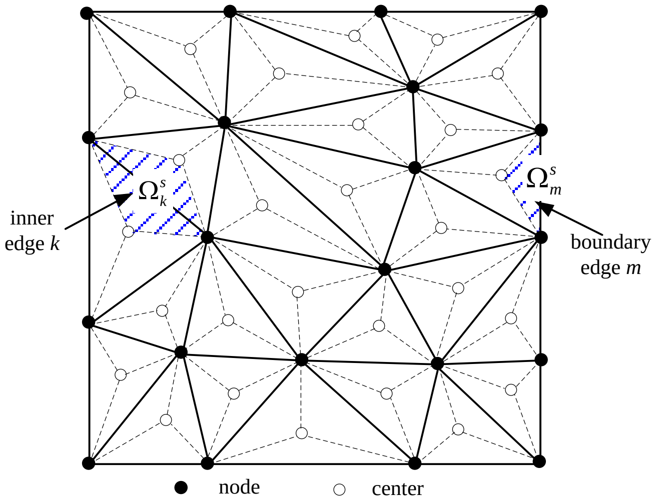

Figure 2. The edge-based gradient smoothing domain for T3 element.

Since ES-FEM for T3 element is highly recommended in solid mechanics, the ES-FEM is first implemented with CBP3 scheme. The gradient smoothing is the fundament of ES-FEM and other S-FEMs. In FEM, the field variables' gradients are calculated by

$$\frac{\partial v_i}{\partial x_j} = \sum_{I=1}^{N_n} \frac{\partial \Phi_I}{\partial x_j} v_{Ii}, \quad \frac{\partial p}{\partial x_j} = \sum_{I=1}^{N_n} \frac{\partial \Phi_I}{\partial x_j} p_I \tag{21}$$

In S-FEM, the gradients of field variables are calculated same with FEM but using smoothed derivatives of shape function

$$\frac{\partial v_i}{\partial x_j} = \sum_{I=1}^{N_n} \overline{\frac{\partial \Phi_I}{\partial x_j}} v_{Ii}, \quad \frac{\partial p}{\partial x_j} = \sum_{I=1}^{N_n} \overline{\frac{\partial \Phi_I}{\partial x_j}} p_I \tag{22}$$

The final equation of the smoothed derivatives of shape function is written as below, more detailed derivation can be found in reference [1]

$$\overline{\frac{\partial \Phi}{\partial x_j}} = \frac{1}{A_i} \sum_{J \in E_i} \Phi(\mathbf{x}_J)\mathbf{n}L_J. \tag{23}$$

where $J \in E_i$ means the J-th edge of smoothing domain Ω_i, L_J is the length of J-th edge, A_i is the area of smoothing domain.

In this paper, the edge-based smoothing domain is used. Its construction is illustrated in **Figure 2**. The edge-based smoothing domain crosses two connecting T3 element which makes the smoothed derivatives of shape function is more smooth than standard derivatives of shape function in whole system. As a result, the ES-FEM, respects to edge-based smoothing domain, for T3 element show softer behavior than FEM using T3 element.

The smoothed weak form of ES-FEM with CBP3 scheme using T3 element (CBP3/ES-FEM-T3) can be written as

$$\begin{bmatrix} \dfrac{M_{IJ}}{\Delta t} + \bar{K}_{IJ} & \bar{G}_{IJi} \\ \bar{G}_{IJi} & V_{IJ} \end{bmatrix} \begin{bmatrix} v_{Ji}^{n+1} \\ p_J^{n+1} \end{bmatrix} = \begin{bmatrix} M_{IJ}\dfrac{v_{Ji}^{n}}{\Delta t} - \bar{C}_{IJ}^{n} v_{Ji}^{n} - \dfrac{\Delta t}{2}\bar{H}_{IJ}^{n} v_{Ji}^{n} + f_{Ii}^{t} + f_{Ii}^{\mathrm{g}} \\ 0 \end{bmatrix} \tag{24}$$

where $\left|\overline{\bullet}\right|$ means smoothed matrices calculated by ES-FEM

$$\begin{aligned}
&[\bar{C}]_{IJ}^{n} = \sum_{l=1}^{N_{ESD}} \int_{\bar{\Omega}_l} \rho\Phi_I \frac{\overline{\partial\left(v_j^n \Phi_J\right)}}{\partial x_j} \mathrm{d}\Omega, \\
&[\bar{K}]_{IJ} = \sum_{l=1}^{N_{ESD}} \int_{\bar{\Omega}_l} \bar{\mathbf{B}}_I^T \mathbf{D}_\mu \bar{\mathbf{B}}_J \mathrm{d}\Omega, [\bar{H}]_{IJ}^{n} = \sum_{l=1}^{N_{ESD}} \int_{\bar{\Omega}_l} \frac{\overline{\partial(v_k^n \Phi_I)}}{\partial x_k} \rho \frac{\overline{\partial(v_j^n \Phi_J)}}{\partial x_j} \mathrm{d}\Omega, \\
&[\bar{G}]_{IJi} = \sum_{l=1}^{N_{ESD}} \int_{\bar{\Omega}_l} \rho\Phi_I \frac{\overline{\partial\left(\Phi_J\right)}}{\partial x_j} \mathrm{d}\Omega, \\
&\bar{\mathbf{B}}_I = \begin{bmatrix} \overline{\dfrac{\partial\Phi_I}{\partial x}} & 0 \\ 0 & \overline{\dfrac{\partial\Phi_I}{\partial y}} \\ \overline{\dfrac{\partial\Phi_I}{\partial y}} & \overline{\dfrac{\partial\Phi_I}{\partial x}} \end{bmatrix}.
\end{aligned} \tag{25}$$

where N_{ESD} is the number of edge-based smoothing domains, $\bar{\Omega}_l$ is the l-th smoothing domain. Above terms' quadrature are approximated using one point area integration at the center of smoothing domain.

Numerical example

Taylor-Green vortex

The Taylor-Green vortex problem is a benchmark with following analytical solution [13],

$$\begin{cases} v_x = \sin(x)\cos(y)\exp(-2\dfrac{\mu t}{\rho}), \\ v_y = -\cos(x)\sin(y)\exp(-2\dfrac{\mu t}{\rho}), \\ p = \dfrac{\rho}{4}\left[\cos(2x) + \cos(2y)\right]\exp(-4\dfrac{\mu t}{\rho}). \end{cases} \tag{26}$$

The analytical solution of Taylor-Green vortex problem is a unsteady solution which is desire to verify the CBP3 scheme.

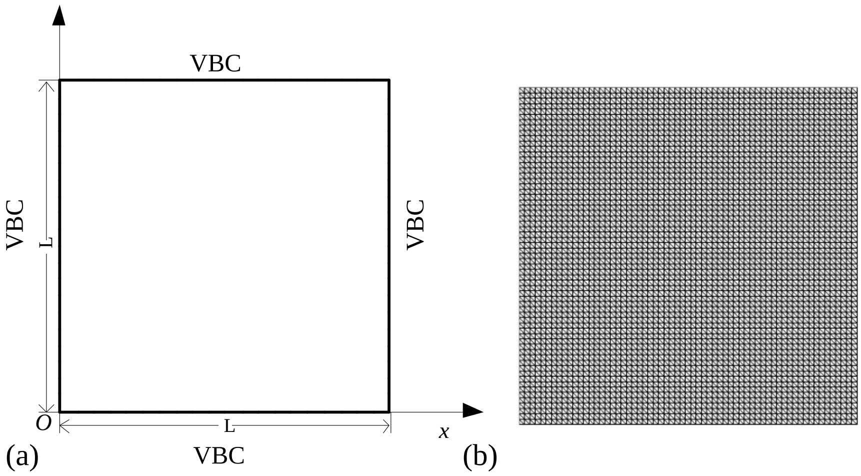

Figure 3. The edge-based gradient smoothing domain for T3 element.

The fluid domain for Taylor-Green vortex is a square with $\mathrm{L}=2\pi$ m , plotted in **Figure 3**(a). A set of uniform meshes, with characteristic element length h=0.4 m, h=0.3 m, h=0.2 m and h=0.1 m, is used to test the convergence of CBP3/FEM-T3 and CBP3/ES-FEM-T3. In (b), the mesh with h=0.1m is plotted. The total computation time is *t*=3s, the time step length is 0.1s for both methods. The fluid density is is 1 kg/m^3, the fluid dynamic viscosity μ is 0.1 kg/(m·s). The stabilization parameter $\alpha=1$, according to reference [8]. The initial conditions and boundary conditions are prescribed as the analytical solution in Eq.(26).

In **Figure 4**, the v_x contours of Taylor-Green vortex problem calculated by CBP3/FEM-T3 and CBP3/ES-FEM-T3 are presented. Two proposed methods give almost identical v_x contours without visible oscillation. The same situation is happened for the pressure contours , see

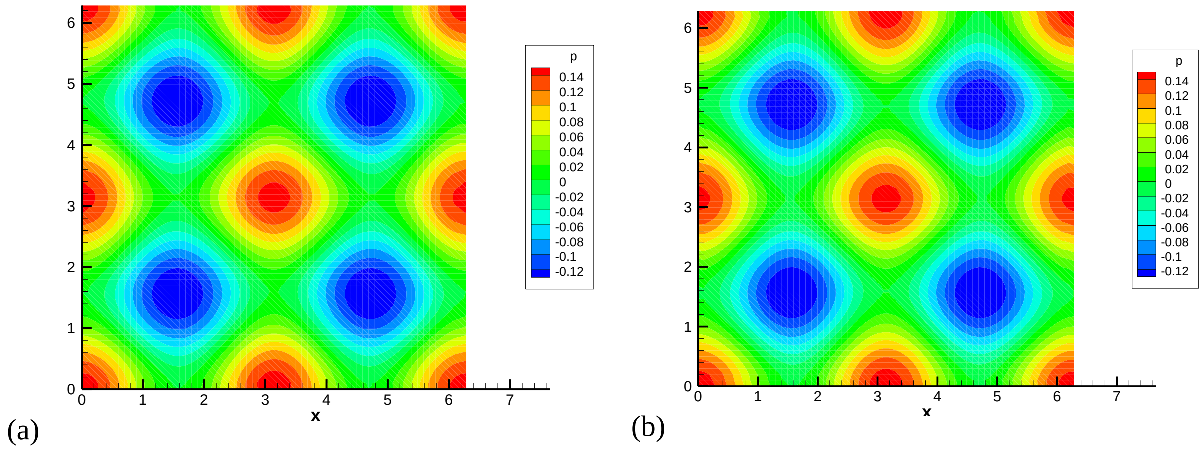

Figure 5.

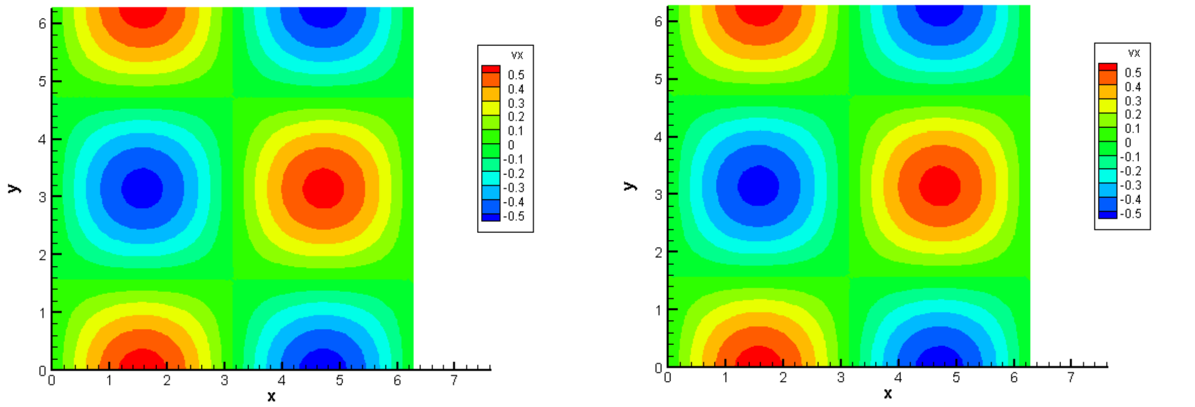

(a) (b)

Figure 4. The contours of v_x for CBP3/FEM-T3 (a) and CBP3/ES-FEM-T3 (b).

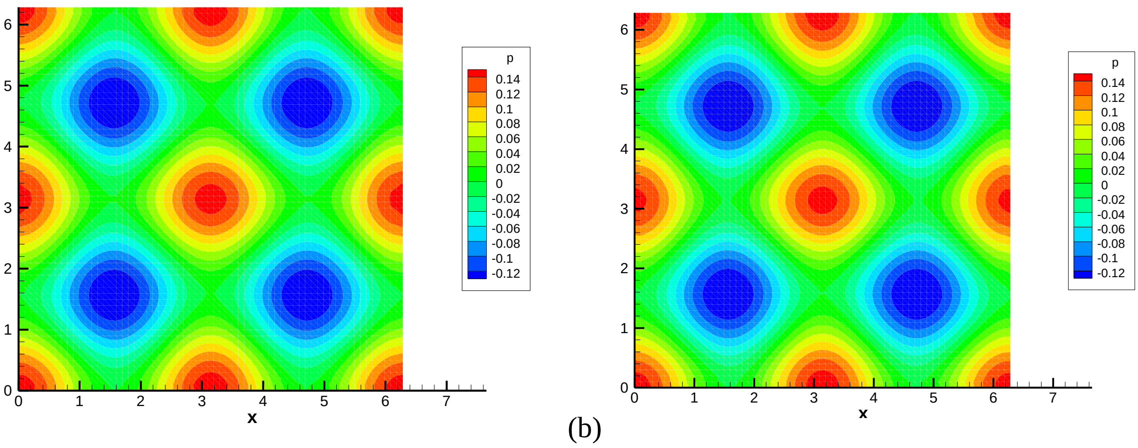

(a) (b)

Figure 5. The contours of *p* for CBP3/FEM-T3 (a) and CBP3/ES-FEM-T3 (b).

As a further investigation, the absolute errors of v_x ($\left|v_x - v_x^{analytical}\right|$) on all node are calculated and plotted as contours in

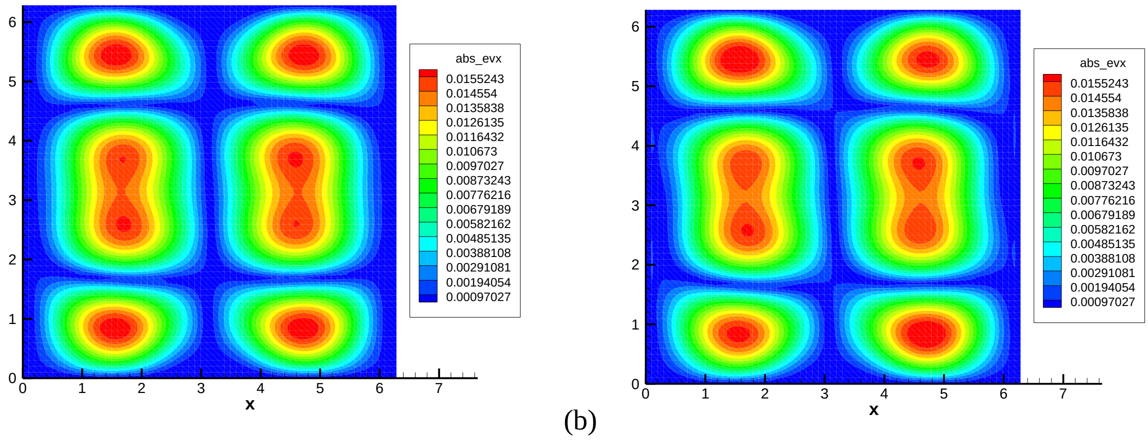

(a) (b)

Figure 6. CBP3/ES-FEM-T3 exhibits slightly better results at areas near the line y=3m. Likewise, the absolute nodal pressure errors are also plotted as contours in

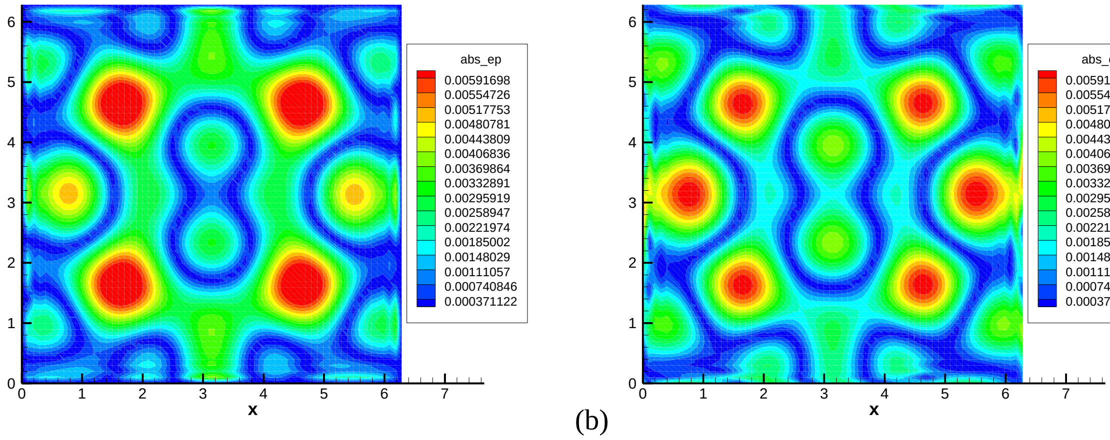

(a) (b)

Figure 7. The errors distributed in problem domain share resemblance for CBP3/FEM-T3 and CBP3/ES-FEM-T3. But it is obvious that CBP3/ES-FEM-T3 has a better pressure accuracy.

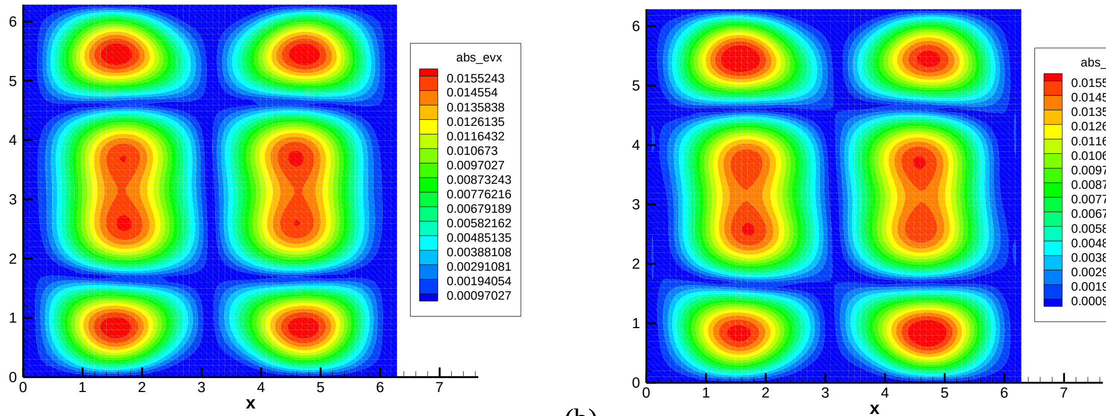

(a) (b)

Figure 6. The contours of absolute error of v_x for CBP3/FEM-T3 (a) and CBP3/ES-FEM-T3 (b).

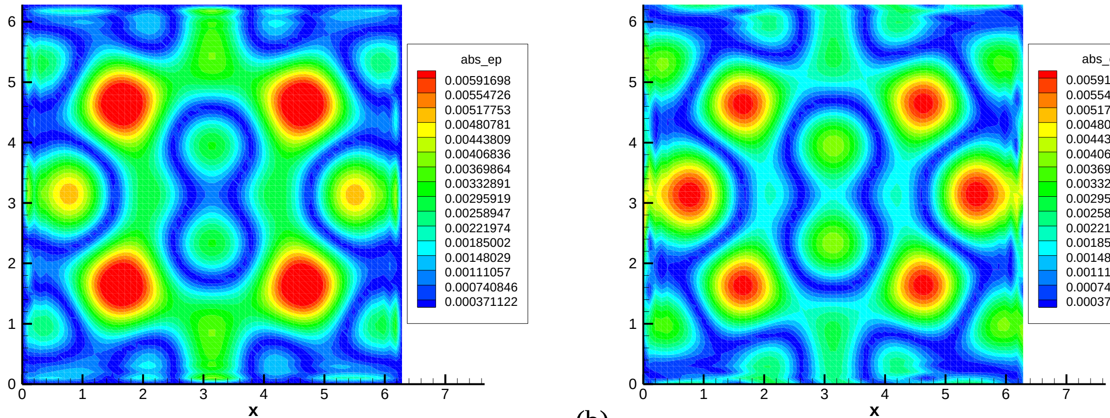

(a) (b)

Figure 7. The contours of absolute error of p for CBP3/FEM-T3 (a) and CBP3/ES-FEM-T3 (b).

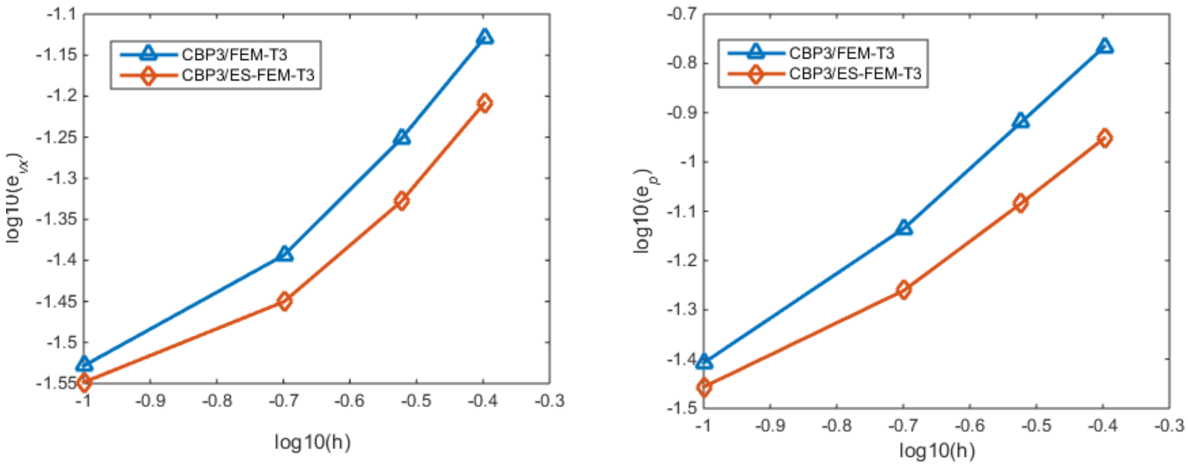

(a) (b)

Figure 8. The spatial convergence of v_x (a) and p (b) for CBP3/FEM-T3 and CBP3/ES-FEM-T3 ($\Delta t = 0.1s$, $\alpha = 1$).

The spatial convergence studies of CBP3/FEM-T3 and CBP3/ES-FEM-T3 are conducted on v_x and p. The L2 norms of errors of v_x and p are used as accuracy indicator. The convergence curves are obtained on meshes with characteristic element length h=0.4 m, h=0.3 m, h=0.2 m and h=0.1 m. In **Figure 8**, convergence curves of v_x and p are drawn. With the contribution of edge-based gradient smoothing, CBP3/ES-FEM-T3 has both better accuracies on velocity and pressure. It is consistent with the absolute errors distributions of CBP3/FEM-T3 and CBP3/ES-FEM-T3 in **Figure 6** and **Figure 7**.

The temporal convergence is also studied. Here, four time steps, $\Delta t = 0.1\text{s}$, $\Delta t = 0.05\text{s}$, $\Delta t = 0.025\text{s}$, $\Delta t = 0.0125\text{s}$ and $\Delta t = 0.00625\text{s}$, are selected for CBP3/FEM-T3 and CBP3/ES-FEM-T3 using mesh with 1024 nodes and h=0.2m. The calculated L2 norms of errors of v_x and p are plotted in **Figure 9**. In all different time step circumstances, CBP3/ES-FEM-T3 is superior than CBP3/FEM-T3.

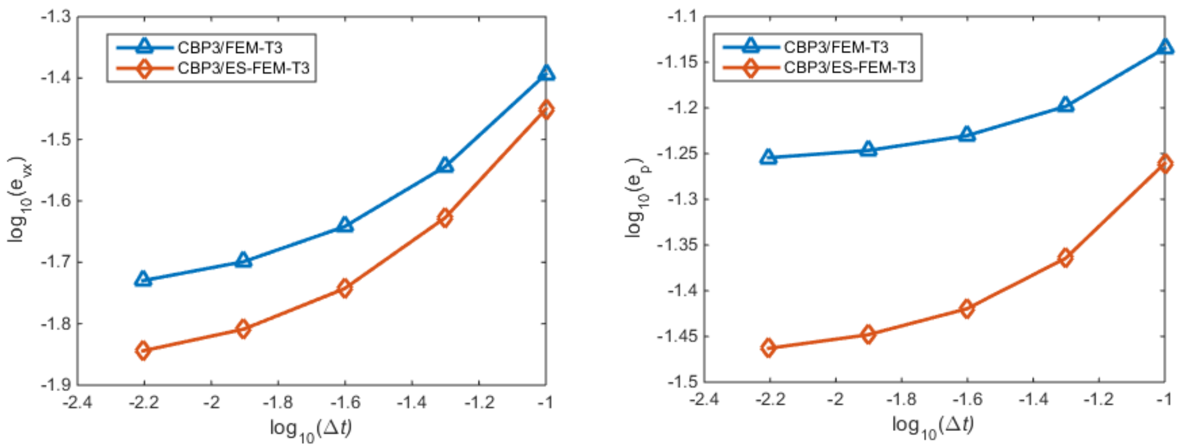

(a) (b)

Figure 9. The temporal convergence of v_x (a) and p (b) for CBP3/FEM-T3 and CBP3/ES-FEM-T3 (1024 nodes, $\alpha = 1$).

Conclusions

A new CBP3 stabilization scheme is developed in this paper. This CBP3 has also been implement into FEM and ES-FEM using T3 element. The convection oscillations of FEM and S-FEM are reduced by characteristic-based method. The pressure calculation in CBP3 for incompressible flow is no longer by solving the pressure Poisson equation of previous CBS algorithm. The CBP3 calculates pressure by polynomial pressure projection method whose equation only relates to shape function. The numerical example, Taylor-Green vortex, are employed here as a verification. Despite that the Reynolds number is only 10, the numerical example still demonstrated proposed CBP3 scheme is able to help FEM-T3 to solve incompressible laminar flows. Besides, with this proper stabilization, ES-FEM-T3 is proved its capability for computational fluid dynamics. Meanwhile, the edge-based gradient smoothing can boost the ES-FEM-T3 with better accuracy than FEM-T3. From this very primitive study, ES-FEM-T3 can be concluded as a better choice for incompressible flow simulation using unstructured T3 mesh.

Acknowledgements

The corresponding author also appreciates the support of the National Natural Science Foundation of China (No. 11232004) and Specialized Research Fund for the Doctoral Program of Higher Education, China (No. 20130161130001).

References

[1] Liu GR., Trung NT. (2010). Smoothed Finite Element Methods [Internet]. Boca Raton: CRC Press;

[2] Liu GR., Nguyen-Thoi T., Lam KY. (2009). An edge-based smoothed finite element method (ES-FEM) for static, free and forced vibration analyses of solids. *J Sound Vib*. **320**(4–5):1100–30.

[3] He ZC., Li GY., Zhong ZH., Cheng a. G., Zhang GY., Liu GR., Li E., Zhou Z. (2012). An edge-based smoothed tetrahedron finite element method (ES-T-FEM) for 3D static and dynamic problems. *Comput Mech*. **52**(1):221–36.

[4] Chen H., Wang Q., Liu GR., Wang Y., Sun J. (2016). Simulation of thermoelastic crack problems using singular edge-based smoothed finite element method. *Int J Mech Sci*. **115**–**116**:123–34.

[5] Nguyen-Xuan H., Liu GRR. (2013). An edge-based smoothed finite element method softened with a bubble function (bES-FEM) for solid mechanics problems. *Comput Struct*. **128**:14–30.

[6] Zienkiewicz OC., Taylor RL., Nithiarasu P. (2014). The Finite Element Method for Fluid Dynamics [Internet]. Finite Elem. Method Fluid Dyn. Elsevier;

[7] Zienkiewicz OC., Codina R. (1995). A general algorithm for compressible and incompressible flow—Part I. the split, characteristic-based scheme. *Int J Numer Methods Fluids*. **20**:869–85.

[8] Dohrmann CR., Bochev PB. (2004). A stabilized finite element method for the Stokes problem based on polynomial pressure projections. *Int J Numer Methods Fluids*. **46**(2):183–201.

[9] Zienkiewicz OC., Taylor RL., Nithiarasu P. (2014). 03. The Characteristic-Based Split (CBS) Algorithm: A General Procedure for Compressible and Incompressible Flow [Internet]. Finite Elem. Method Fluid Dyn. Elsevier;

[10] Zienkiewicz, O.C., Loehner, R., Morgan, K., Nakazawa S. (1984). FINITE ELEMENTS IN FLUID MECHANICS: A DECADE OF PROGRESS. *Finite Elem Fluids*. **5**:1–26.

[11] F.Brezzi., Fortin M. (1991). Mixed and Hybrid Finite Element Methods. New York: Springer-Verlag;

[12] Zienkiewicz O., Taylor R., Zhu JZ. (2013). The Finite Element Method: Its Basis and Fundamentals. 7th ed. Oxford: Butterworth-Heinemann;

[13] Taylor, G. I. and Green AE. (1937). Mechanism of the Production of Small Eddies from Large OnesTitle. *Proc R Soc LondonSeries A,Mathematics Phys Sci*. **158**(895):499–521.